Dry Metal Forming Open Access Journal

Fast Manuscript Track

Edited by Frank Vollertsen
Available online at elib.suub.uni-bremen.de

www.drymetalforming.de

Dry Met. Forming OAJ FMT 1 (2015) 42–56
Received 4 February 2015; published 10 February 2015

Investigation of Tribological Systems for Dry Deep Drawing by Tailored Surfaces

Marion Merklein[1], Michael Schmidt[2], Stephan Tremmel[3], Sandro Wartzack[3], Kolja Andreas[1], Tom Häfner[2], Rong Zhao[3], Jennifer Steiner[1]*

[1]Institute of Manufacturing Technology, Friedrich-Alexander-Universität Erlangen-Nürnberg, Egerlandstr. 13, 91058 Erlangen, Germany
[2]Institute of Photonic Technologies, Friedrich-Alexander-Universität Erlangen-Nürnberg, Konrad-Zuse-Str. 3/5, 91052 Erlangen, Germany
[3]Institute of Engineering Design, Friedrich-Alexander-Universität Erlangen-Nürnberg, Martensstr. 9, 91058 Erlangen, Germany

Abstract

Growing ambitions for efficient resource utilization and improving environmental standards stimulate the abandonment of environmentally harmful lubricants. However, dry forming leads to direct contact between tool and workpiece surface which causes increasing friction and wear. This paper presents a methodology for realization of lubricant free deep drawing processes. Dry deep drawing of a rectangular cup is investigated by a numerical simulation. First numerical results reveal the necessity of modifying the tribological system in order to realize dry deep drawing. Basic tribological investigations reveal increasing friction and intensive wear under dry conditions. Therefore, tailored surfaces are developed to improve the tribological properties without lubrication. By laser structuring various micro features were fabricated on the tool surface. Furthermore, tungsten doped hydrogenated amorphous carbon coatings (a-C:H:W) were deposited on the tool using unbalanced magnetron sputtering. The tribological behavior of these surface modifications were researched by a ring-on-disc-tribometer. The wear mechanisms during the dry sliding process are discussed depending on the micro features and coatings. The obtained test results help building the basic concept for generating tailored surfaces and subsequently to realize lubricant free deep drawing.

Keywords: Dry Deep Drawing, Tribology, Laser Generated Micro Features, DLC-Coatings

1 Introduction

Global trends in the forming industry like the demand for efficient usage of resources and a growing environmental awareness motivate the development of green production technologies. One environmental harmful aspect in forming processes is the utilization of frequently mineral oil based lubricants. High efforts are necessary for a proper disposal of the applied lubricants. These aspects motivate the realization of dry forming processes. According to the process chain based definition from Vollertsen et al. [1] dry forming processes are characterized by a workpiece that leaves the forming tool without the necessity of cleaning and drying for subsequent operations like painting or welding. This leads to a reduction of applied resources and process steps. Nevertheless, realizing lubricant free forming operations faces several challenges. The direct interaction between tool and workpiece results in increased friction and wear. To overcome these drawbacks a holistic approach focusing on the tribological mechanisms under dry conditions needs to be applied. The metho-dology to realize dry sheet metal forming processes within the scope of the DFG priority program SPP1676 is shown in Fig. 1 for the project ‘Lubricant free forming with tailored tribological conditions’. The aim of this project is to gain knowledge about the changing tribological conditions and proof the feasibility of lubricant free deep drawing processes. In order to investigate the tribological system laboratory tests are performed. The strip drawing test and the ring-on-disc test were selected as laboratory tests to determine friction and wear. As a reference, lubricated and dry test series were conducted. By varying the testing parameters basic influencing factors are identified. The intensive interaction between tool and workpiece cause high friction and wear. Therefore, surface modifications on the forming tool are necessary. On the one hand side, coatings are applied to reduce the friction. On the other hand side, the tool surface is modified with laser generated structures in order to control the material flow. As model process, deep drawing of a rectangular cup was selected to analyze a

*E-mail address of corresponding author: jennifer.steiner@fau.de

complex state of stress. A numerical model was developed in order to design this dry deep drawing operation and to derive the requirements for the forming tool. Finally, a tailored tool with local adjusted surface properties will be developed in order to realize the model process under dry conditions.

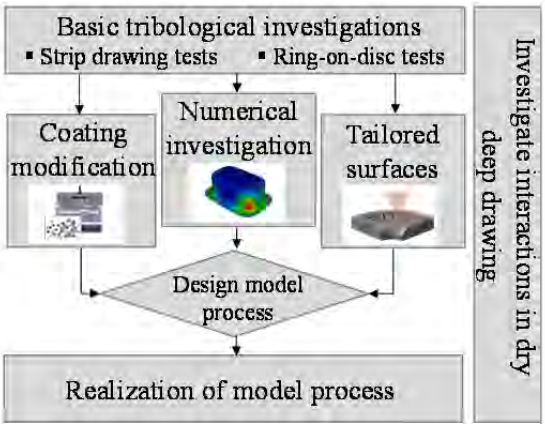

Fig. 1: Project methodology

2 Basic tribological investigations

A first step in order to understand the basic tribological mechanisms is to analyze friction and wear under dry conditions in laboratory tests. The test setup of the selected ring-on-disc and flat strip drawing test will be explained in the following paragraph.

2.1 Setup of ring-on-disc-tribometer

For the ring-on-disc tests a tribometer TRM1000 from the company Wazau is used. The tribological system consists of a unidirectional rotating ring and a sheet metal disc (Fig. 2).

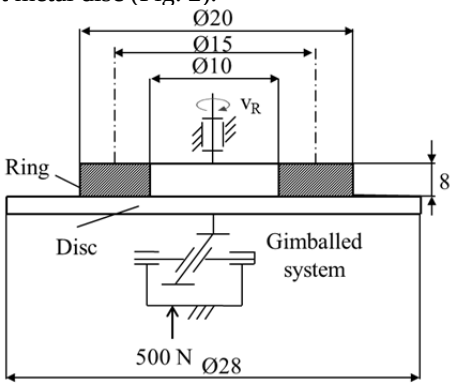

Fig. 2: Principle of the used ring-on-disc-tribometer

The wear behavior of the ring is investigated for long sliding distances at low material consumption by using one ring and a sequence of four single sheets. During the tests axial run-out is provided by the gimballed disc. The dimensions of the inner and outer ring radius are R_I= 5 mm and R_A= 10 mm. For the mean radius R_M= 7.5 mm the rotational speed of v_R= 127 min^{-1} is equal to the usual speed of a punch in deep drawing of v_{rel}= 100 mm/s.

In the ring-on-disc tests the sample size n of every experimental condition is n=3.The ring-on-disc tests are carried out non-lubricated as well as lubricated for the reference experiments. The lubricants Multidraw KTL N 16 from company Zeller+Gmelin and ZO 3368 from company Wisura are used.

The ring-on-disc-configuration allows the investigation of the wear mechanism in dry forming with small material consumption due to the possibility of testing several successive sheets with each ring. The method enables the investigation of the effect of micro features because in comparison to the pin- or ball-on-disc-test the bigger contact area results in over-lapping of several features. Thus, unwanted tilting of the friction partner at the feature edges can be avoided.

The main difference between both test methods is given by the rotational sliding in the tribometer, thus tested and possibly worn surfaces permanently contact each other due to the total number of rotations N ≈ 15. Therefore, worn disc respectively workpiece surfaces are facing the ring or tool surface over a longer run within this closed tribological system than in the open tribological systems of the flat drawing strip test and the deep drawing process. For this reason, the level of abstraction of the ring-on-disc-test is higher than the one of the flat strip drawing test regarding deep drawing processes.

2.2 Setup of flat strip drawing test

The flat strip drawing test is commonly used to determine friction coefficients for deep drawing processes [2]. Fig. 3 shows the basic principle of the applied test setup. The analyzed tool-workpiece interface consists of an upper, fixed friction jaw, a sheet metal strip and a lower, moving friction jaw. The sheet metal strip is placed between the friction jaws. The lower jaw is moving upwards in order to apply a defined normal force F_N. While the strip is drawn through the friction jaws with a distinct drawing velocity v_{rel}, the resulting friction force F_F is measured.

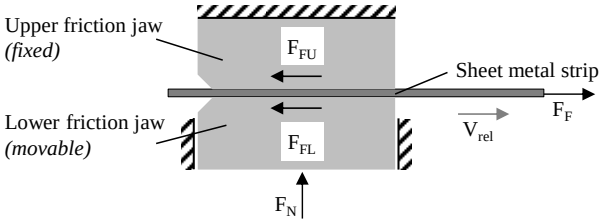

Fig. 3: Setup of flat strip drawing test

The friction coefficient μ is determined by the Coulomb friction law according to eq. (1). Because of the two sided contact only half of the friction force has to be considered.

$$\mu = (F_F / 2) / F_N \quad (1)$$

The total drawing length is 190 mm. The evaluation area is set between 100 and 170 mm to eliminate the influence of starting and slowing down process. This test setup enables the investigation of friction coefficients of numerous tribological conditions by varying the normal load, the drawing velocity and the lubricational conditions.

2.3 Results of reference tests

The reference strip drawing tests were carried out for the deep drawing steel DC04 and the aluminum

alloys AA6014 and AA5182 with a sheet thickness of 1 mm. As tool material the cold working steel 1.2379 was applied. For better comparison all sheet metal materials have an electrical discharge texture (EDT). In order to prevent corrosion during transport and storage the sheet material receives a basic lubrication. Additionally, the DC04 sheet has a zinc coating as corrosion protective layer. Before strip drawing tests are performed, all strips are cleaned with acetone in order to remove the basic lubrication. The oil film sensor NG from the company Infralytic is used to control the surface cleaning. For each strip 5 points on each side are measured. The cleaning process is repeated until the oil film thickness is equal 0.0 g/m². Afterwards, oil is applied manually by a foam roll for lubricated test series. According to typical lubrication amount for car body parts, the oil film thickness is chosen to m = 2.0 g/m² [3]. Once again 5 points on each strip side are measured with the oil film sensor in order to monitor the homogeneity and amount of the applied oil. The friction jaws were machined by combined grinding and finishing. After grinding, the tools were first lapped and then polished with an oil based diamond suspension with a grain size of 9 µm. In order to assure equal testing conditions, a surface characterization of the tool surface was conducted before each test. Fig. 4 shows the dimension of the friction jaws and the initial topography before the strip drawing test. The measurement was performed with the confocal microscope µSurf from NanoFocus. After lapping and polishing all grinding marks are eliminated. This results in a smooth surface without preferential direction.

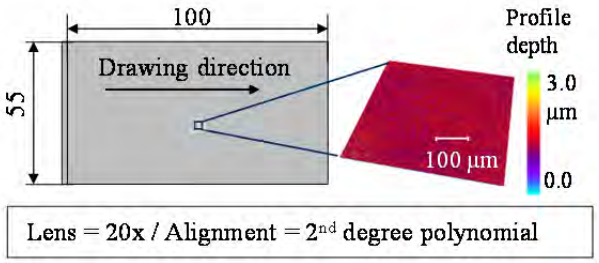

Fig. 4: Geometry and initial topography of friction jaws

Some pre-investigations were performed in order to choose the reference lubricant and to quantify the level of the friction coefficient under dry conditions. The lubricated tests are performed as a reference for the changing tribological properties under dry conditions. The dry experiments are conducted to determine the general friction level without lubrication. The three different oils AK 3080 and ZO 3368, both from Wisura, and KTL N 16 were selected for the lubricated test series. AK 3080 and ZO 3368 are high performance oils for minimum quantity lubrication. They are generally used for varying forming processes in particular with aluminum alloys. The lubricant Multidraw KTL N 16 is a high performance lubricant especially developed for deep drawing operations. Furthermore, it is approved for the application in automotive industry by the German Automotive Industry Association.

The resulting friction coefficients are depicted in Fig. 5. The values for the friction coefficients vary between 0.03 and 0.59 depending on the lubrication and the sheet metal material. The experiments with DC04 lead to an increase of friction between the lubricated and dry strips of approximately 250 %. Analyzing the test series with AA5182 there is a friction increase from approximately 0.03 under lubricated to 0.3 under dry conditions. An even higher rise of friction occurs for AA6014. The friction coefficient of the dry tests is approximately 20 times higher than the value under lubricated conditions. The strips lubricated with AK 3080 lead to the highest friction under lubricated conditions. Reason might be that AK 3080 has the lowest viscosity and therefore the oil can be easily squeezed out of the contact zone between jaw and strip. KTL N 16 leads to friction coeffi5182cients between the values for AK 3080 and ZO 3368. KTL N 16 has a high viscosity of 160 mm²/s. This improves the homogeneity and handling of the manual oil application process. KTL N 16 will be used in further test series as reference lubricant because it reflects the mean friction level with lubrication and guarantees an improved oil application due to higher viscosity.

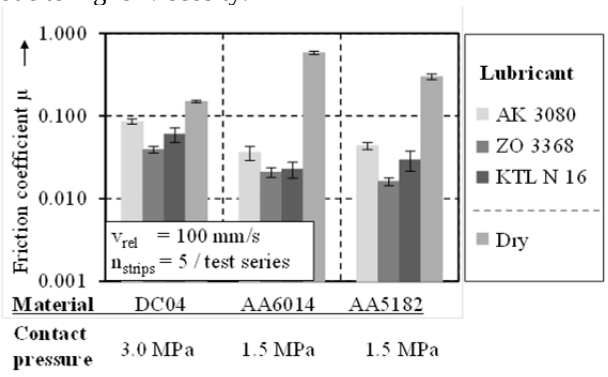

Fig. 5: Comparison of friction coefficient for several lubricated and dry test series

Using conventionally lubricated strips the friction coefficients reach roughly the same levels for all material. As shown in Fig. 5 under lubricant free conditions the friction coefficients vary extremely depending on the different sheet materials. The dry friction coefficient approximately doubles from DC04 to AA5182 and doubles again to AA6014. Employing these materials in a forming process will lead to different retention force in the flange area between blank holder and sheet. This fact will be considered in the further strip drawing tests by using different levels of contact pressure for each material.

In order to gain knowledge about the friction and wear mechanisms under dry conditions several test series were performed. As already known from former investigations under lubricated conditions the main factors influencing the friction coefficient are the velocity, the lubricational conditions and the contact pressure [4]. In the following experiments, the strip drawing tests were conducted at drawing velocities of 50 mm/s, 100 mm/s and 150 mm/s. Furthermore, the contact pressure is varied in two steps for the dry tests. To have a reference for conventional conditions, additionally lubricated test series were carried out. Tab. 1 summarizes the experimental parameters for

each material. AA6014 is analyzed like DC04 under dry conditions in a full factor experimental design. For the two aluminum alloys similar tribological behavior is expected therefore AA5182 is investigated at constant drawing velocity and contact pressure.

Tab. 1: Investigated parameters for basic strip drawing tests

Sheet material	Lubrication (g/m²)	Drawing velocity (mm/s)	Contact pressure (MPa)
DC04	0.0 (dry)	50 / 100 / 150	1.5 / 3.0
	2.0 (KTL N 16)	50 / 100 / 150	1.5
AA6014	0.0 (dry)	50 / 100 / 150	1.0 / 2.0
	2.0 (KTL N 16)	50 / 100 / 150	1.0
AA5182	0.0 (dry)	100	2.0
	2.0 (KTL N 16)	100	2.0

Fig. 6 depicts the resulting friction coefficients for the varying test parameters. Looking at the test series for DC04 a slight reduction of friction coefficient occurs when the higher contact pressure of 3 MPa is applied. An explanation for this might be the low hardness and strength of soft zinc coatings [5]. At higher pressure the plastic deformation of the zinc layer increases. Due to this deformation zinc asperities are smoothened and fill the rough spots on the surface as described in [6] for lubricated strip drawing tests. Therefore, the resistance to sliding motion is reduced. Other studies investigating the tribological behavior of various zinc layers confirmed that a small amount of zinc wear debris might function as solid lubrication [7]. These effects need to be investigated in further experiments especially for dry conditions.

Evaluating the results of the AA6014 strips this effect does not reveal. In contrast, a slight increase of the friction coefficient occurs under higher contact pressure. A reason might be that the wear is caused by galling. A higher contact pressure leads to smoothening and a growing area of true contact. Thus, the target area for adhesion occurrence increases. Comparing the friction coefficients at different drawing velocities no significant influences reveal. This leads to the conclusion that the drawing velocity at the chosen stages under lubricantfree conditions has no impact on the friction level. The dependency between velocity and friction is mainly caused by hydrodynamic effects of the lubrication. For the lubricated test series with DC04 the friction tends to decrease with increasing drawing velocity. According to the Stribeck curve the friction coefficient does not depend on the velocity during solid friction [8]. Besides, Coello et al. [9] stated, that the influence of sliding velocity on the friction coefficient depends on the contact pressure. The impact increases with increasing contact pressure and is not detected at low pressures. With this test setup the reachable contact pressure under dry conditions is limited to the tensile strength of the strip material. Thus, it seems reasonable that the results of the dry test series show no significant correlation between velocity and friction coefficient. The friction coefficient for DC04 under dry conditions tends to decrease slightly for increasing velocity. In contrast for AA6014 no distinctive changes of the friction coefficients reveal for varying velocity.

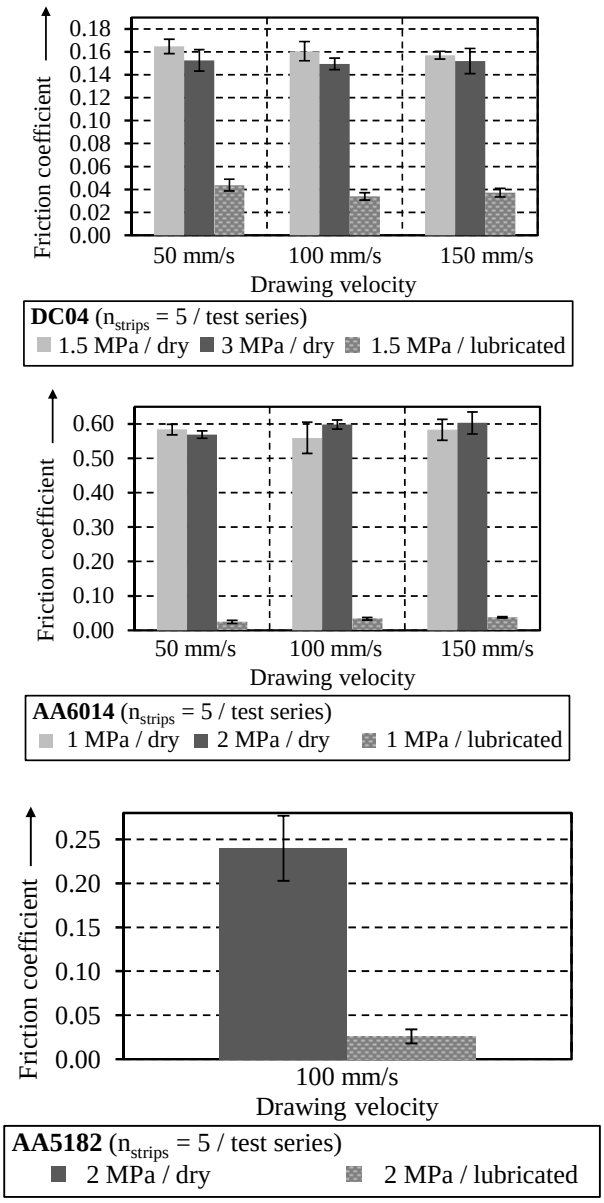

Fig. 6: Friction coefficients for DC04, AA6014 and AA5182

In order to find reasons for the huge deviations between the friction coefficients for the different materials a surface characterization was performed prior and after testing. A comparison of the sheet topography is given in Fig. 7. For each material 30 measurements were conducted by confocal microscopy on a µSurf. For each material an exemplary surface topography is shown. The three materials have an EDT surface. Nevertheless, the topography of DC04 reveals a different structure than the two aluminum alloys. A reason might be different material behavior and the zinc coating on the DC04 surface. DC04 has a higher profile depth and more flattened peaks which lead in average to a higher arithmetic mean roughness Sa of 1.5 µm but a lower reduced peak height Spk of 0.7 µm compared to AA6014 and AA5182. The roughness averaged over 30 measurements for the two aluminum alloys is on the same level. However, looking at the reduced peak height Spk AA6014 has 35 % higher average peak height. These peaks might lead to an interlocking of the

asperities with the tool surface. This effect explains why the friction coefficient under dry conditions is much higher for AA6014 than for AA5182.

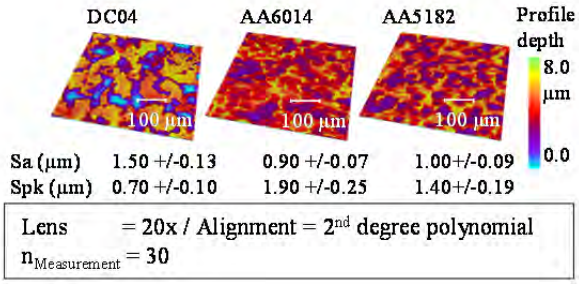

Fig. 7: Initial surface topography of sheet metal strips

The surface of a friction jaw and exemplarily topographies after drawing 5 strips under lubricant free conditions are depicted in Fig. 8. The tests were performed with a velocity of 100 mm/s and a contact pressure of 3 MPa for DC04 and 2 MPa for the aluminum strips. In the former test setup for lubricated experiments the strips had width of 30 mm and the frictions jaws had a width of 55 mm. Thus the cutting edge of the strips was within the contact zone. Under dry conditions this leads to intensive wear along the edge. Thus the width of the strips was changed to 65 mm to ensure that the cutting edges are not in contact with the friction jaws. The friction jaws which were used in the tests with DC04 and AA5182 reveal no significant wear. Compared to the initial tool topography shown in Fig. 4 no surface changes occur. Looking at the friction jaw which was in contact with AA6014, extensive wear in form of adhesion occurs. The topography of measuring area b) shows this in detail. Surface peaks of AA6014 interlock with the surface roughness of the friction jaws. When the shear stresses exceed the material strength some sheet surface particles are transferred to the tool surface. This process increases the resistance to the sliding motion and therefore increases the friction coefficients. Thus, the results of the surface characterization agree with the results of the strip drawing test.

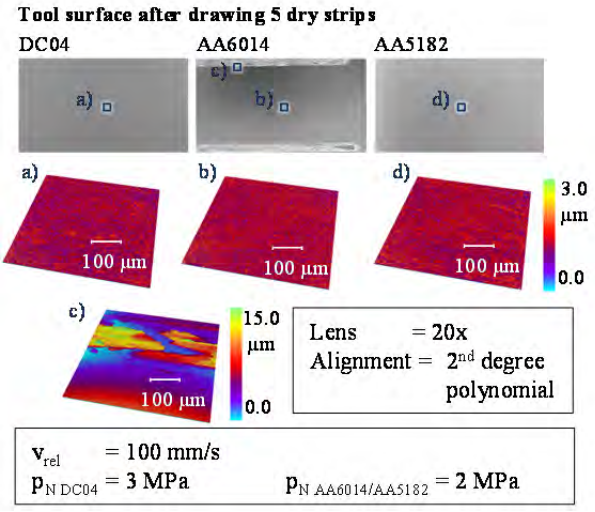

Fig. 8: Comparison of tool topography after strip drawing test

In addition, Fig. 9 presents exemplary strip surfaces after drawing. These strips were tested under dry conditions at a drawing velocity of 100 mm/s and a contact pressure of 3 MPa for DC04 and 2 MPa for the aluminum alloys. Compared to Fig. 7 the surface of DC04 is smoother. The size and depth of the roughness valleys of the zinc layer appear less distinctive than before testing. This effect seems to reinforce the explanation for the decrease of friction when the contact pressure increases for DC04. For AA6014 two surface measurements are depicted in Fig. 9 to visualize the intensive interaction between tool and workpiece which lead to high friction coefficients. As already shown in Fig. 8 adhesive wear only appears locally. Therefore, the sheet topography is smoothened at some areas whereas others reveal a much higher roughness than before testing. Comparing the results in Fig. 7 and Fig. 9, the surface flattening for AA5182 is not as intense as for DC04. Reason might be the lower contact pressure and different hardness of the surface layers.

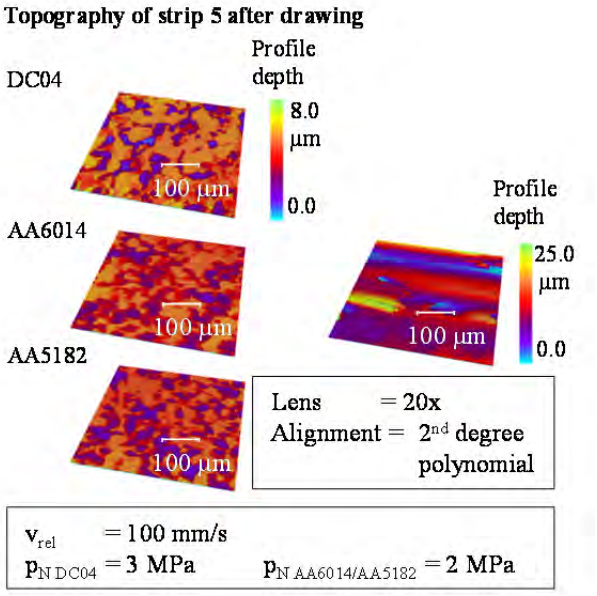

Fig. 9: Comparison of sheet topography of strip 5 after drawing

3 Modell process

Within this project a rectangular cup deep drawing process should be realized under lubricant free conditions. The basic process and workpiece geometry is shown in Fig. 10. The rectangular cup has a width of 53 mm and a length of 93 mm.

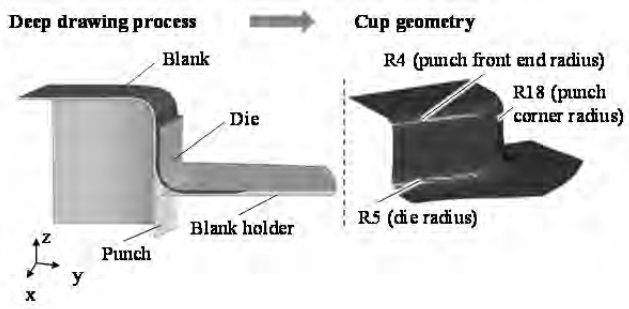

Fig. 10: Investigated deep drawing process and cup geometry

3.1 Description of numerical Model

The forming process is modelled in the FE-Software LS Dyna R7. The symmetry of the workpiece is used to reduce the computation time by generating a 90°-model. The scope of the numerical investigation is to identify critically loaded tool segments in order to design the forming process according to the requirements of dry deep drawing. Before modelling the forming process basic input parameters are experimentally determined. A DC04 and the aluminum alloys AA6014 and AA5182 with a sheet thickness of 1 mm are used as workpiece material. A material characterization was performed in order to derive the stress-strain curve, the yield surface and the forming limit curve. Fig. 11 summarizes the experimental results of corresponding tensile tests, biaxial tensile tests and Nakajima-tests. Comparing the three materials, the different material properties between the deep drawing steel and the aluminum alloys become obvious. As a yield criterion the material model of Barlat 2000 [10] is used for all materials. The yield surface shows the transition from elastic to plastic material behavior under multi-axial strain conditions. DC04 has a more elliptical and elongated shape which means that higher stresses are necessary to achieve plastic deformation. According to the Hockett-Sherby approximation which is commonly used in forming simulations for the stress-strain curves [11] all materials obtain a nearly constant true stress level starting at a strain value of 0.4. DC04 reaches a higher stress level up to a yield stress of 400 MPa. AA6014 and AA5182 have nearly the same maximum yield stress level between 330 and 350 MPa. In Fig. 11 (c) the forming limit curves for DC04, AA5182 and AA6014 are presented. When major and minor strain exceed the forming limit curve material failure in terms of cracks occurs. AA5182 and AA6014 have forming limit curves of a similar level whereas DC04 achieves a much higher formability level.

Besides the material input parameters, the friction coefficients are necessary. Tab. 2 shows the applied friction coefficients for the different material combinations. The values are set according to a conservative approximation resulting from the strip drawing tests.

Tab. 2: Utilized friction coefficients

Tool material	Workpiece material	Lubricational conditions	Friction coefficient
1.2379	DC04	dry	0.20
1.2379	AA5182	dry	0.30
1.2379	AA6014	dry	0.57

Furthermore, the geometry needs to be defined. Therefore, the CAD data is imported as IGES-file. The tools are implemented as rigid bodies because the loads in sheet metal forming operations are too low to cause a tool deformation. Blank and tools are modelled with quadrilateral shell elements in order to enable homogenous meshing. The blank has an average element size of 1.25 mm.

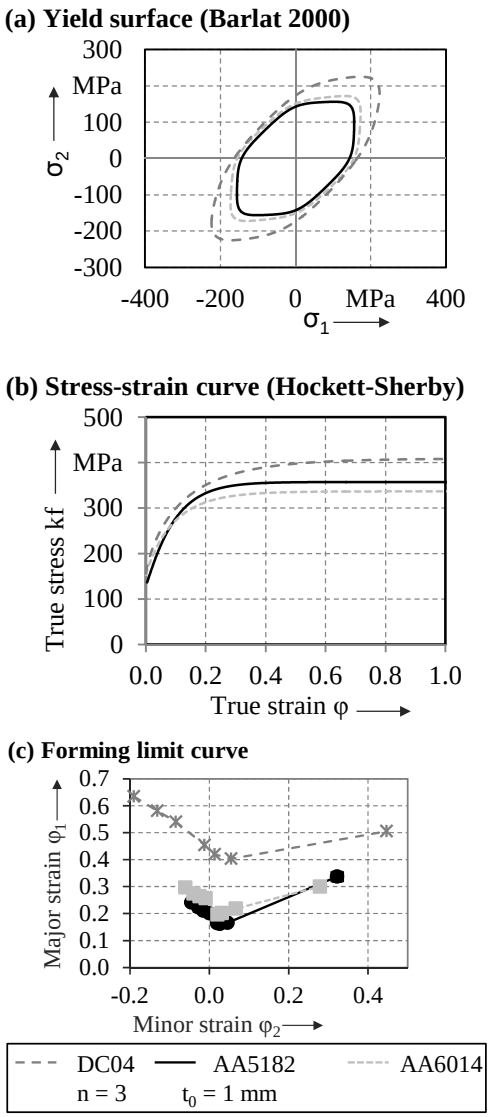

Fig. 11: Results of material characterization for DC04, AA5182 and AA6014 - (a) stress-strain curve, (b) yield function and (c) forming limit curve

3.2 Design of variant simulation

In order to gain process knowledge and identify the main influencing parameters in dry deep drawing a variant simulation is conducted. In conventional lubricated drawing processes, the limiting process parameters are sheet material, punch and die radii, blank holder forces, drawing gap and friction [12]. Prior numerical investigations have shown negligible influence of the drawing gap within the recommended range on the tool load and drawing ratio. Therefore, the drawing gap is set to the fixed value of 1.4 mm. The friction coefficients are derived from the experiments and will not be varied for within basic investigations. The numerical results will be used to define the requirements for the development of surface modifications. Later in this project the friction coefficients for the tailored surfaces will be implemented in order to develop a segmented tool. Hence, the parameters tool geometry, blank holder force and sheet material will be analyzed. A full factor experimental design is applied for the variant simulation

to evaluate also the dependencies between these parameters. Tab. 3 summarizes the values for the varied tool radii. For each radius three grades will be investigated. The punch front end radius was varied between 3.0 mm and 5.0 mm. Smaller radii lead to higher tool loads. Therefore, the values were set on a low level to proof the feasibility of dry deep drawing under practical relevant conditions.

Tab. 3: Variation of geometrical tool parameters

Punch front end radius (mm)	3.0	4.0	5.0
Punch corner radius (mm)	18.0	20.0	22.0
Die radius (mm)	2.5	5.0	10.0

Furthermore, the blank holder force has an influence on the material flow and the deep drawing result. The blank holder forces presented in Tab. 4 refer to the 90° model. The diverse friction coefficients and material properties lead to different force levels for each sheet material. DC04 has the lowest friction coefficient. Therefore a higher blank holder force is necessary to achieve the same retention force. Consequently, the lowest blank holder forces are applied for AA6014 which is related to the highest friction coefficients.

Tab. 4: Variation of blank holder forces for each sheet material

Sheet material	Blank holder forces (kN)		
DC04	3.00	6.00	9.00
AA5182	1.50	2.00	2.50
AA6014	0.75	1.00	1.25

The three sheet materials have different formabilities as depicted in Fig. 12 and encounter diverse tribological conditions. Therefore, the limiting draw ratio achieved for each material varies in a wide range. This has to be considered when the blank geometry is designed. Within an upfront numerical investigation the design of the blank was defined. Fig. 12 shows the blank dimension and the achievable cup height exemplarily for the punch front end radius of 4.0 mm, the corner radius of 18.0 mm and a die radius of 5.0 mm at the medium blank holder force level. In general a rectangular geometry with 45° cutoff edges was selected. The size depends on the sheet material. DC04 with its higher formability and lower friction reaches the highest drawing ratio and has therefore a bigger blank geometry than AA6014 and AA5182. Thus, the cup height achieves a value of 21.0 mm compared to 11.0 mm for AA6014 and 14.0 mm for AA5182.

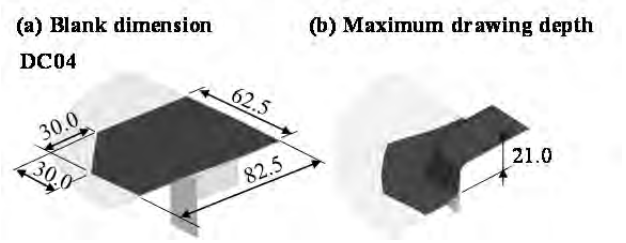

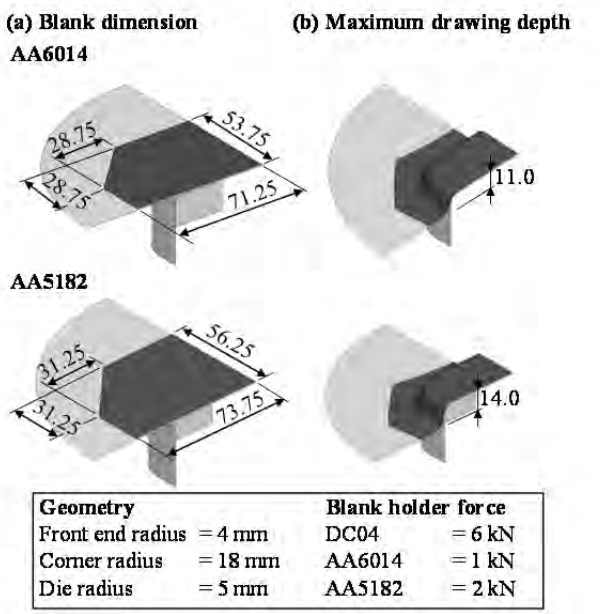

Fig. 12: (a) selected blank dimension and (b) resulting maximum drawing depth for DC04, AA6014 and AA5182

3.3 Numerical results

In the following some exemplary numerical results are presented comparing the three materials. The results shown here refer to the punch front end radius of 4.0 mm, the corner radius of 18.0 mm and a die radius of 5.0 mm at the medium blank holder force level. Fig. 13 compares the contact pressure at the punch at the final forming stage. High tool loads are concentrated at the corner of the punch front end radius. The distribution is similar for all sheet materials. Higher punch forces are necessary to form the DC04 blank. Therefore, the highest tool loads result when using DC04 with maximum contact pressure of 130 MPa. Nevertheless, the relative motion between punch and sheet is negligible which means that this section is not that wear-critical.

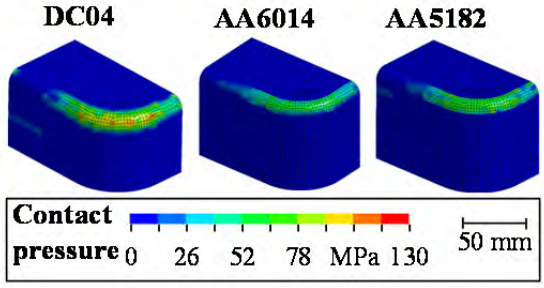

Fig. 13: Comparison of contact pressure at the punch

In contrast, between the die and the sheet surface more relative motion occurs. Therefore, especially the design of the die transition needs to be considered when developing a tailored tool for dry forming. Fig. 14 depicts the contact pressure at the die for the forming operations with DC04, AA6014 and AA5182. First, differences in the level of the resulting contact pressure reveals. The highest contact pressure with a maximum value of 105 MPa occurs when forming DC04. The level of contact pressure is lower for forming AA5182 and AA6014. Reason for the different tool loads at

punch and die when comparing the three materials are different process forces. The forming force for DC04 reaches a maximum value of 16.5 kN. For AA6014 and AA5182 the maximum punch forces are 14.0 kN and 12.5 kN. Similar for all three sheet materials is the general distribution of the contact pressure. Critical tool loads are concentrated in the radius of the die. The highest loads occur in the corner of the die radius. Especially this tool areas need to be segmented and modified by tailored surface properties.

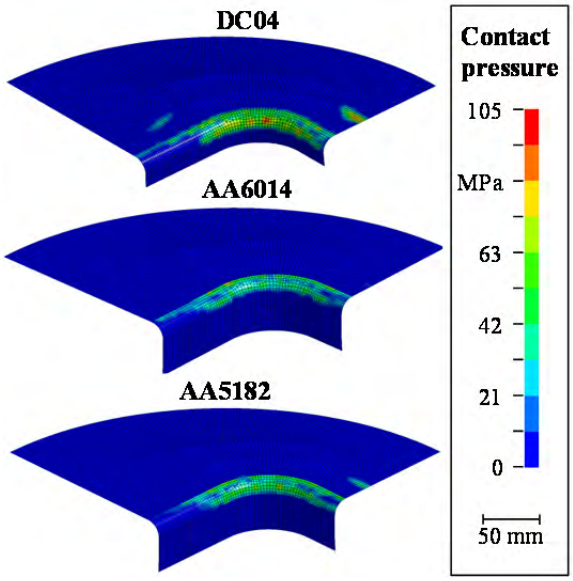

Fig. 14: Comparison of contact pressure at the die

The numerical results reveal a high tool load in the die radius and low drawing depth especially for the aluminum alloys with high friction coefficients. Modifications of the forming tool are necessary in order to reduce wear and increase the drawing ratio. One approach to develop a tailored tool for dry forming is the application of tailored surfaces. The tribological behavior of these surface modifications will be presented in the following.

4 Investigation of tailored surfaces

The results of dry strip drawing tests as well as first numerical results show the challenges of lubricant free forming processes. The intensive interaction between tool and workpiece leads to increasing friction and adhesive wear. The properties of topography and roughness are important influencing parameters when tool and blank surface are in direct contact. The tribological behavior of several surface adjustments is investigated in order to identify surface modifications which decrease the adhesion tendency.

4.1 Influence of varying topography structures

Within strip drawing tests the influence of tool roughness and surface structure were analyzed. The tool surfaces were finished by grinding or polishing with different process parameters. For the grinding process a CBN wheel was used to achieve a smooth ground surface and a corundum wheel was used for the rougher surface. The tools were ground in 0° and 90° degree referring to the drawing direction. The polishing process leads to a smooth surface without preferential direction. Fig. 15 shows the investigated topographies of the friction jaws and the averaged roughness height Rz. The rough ground friction jaws have a raw surface with a high profile depth. Both, the rough and smooth ground tools have a preferential direction while the polished friction jaws reveal an even smoother and undirected surface structure.

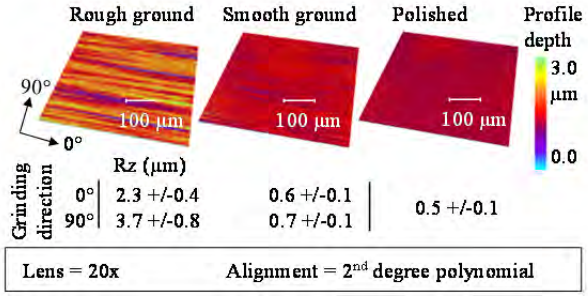

Fig. 15: Initial tool topography and Rz values

Within the strip drawing test the friction coefficients are determined under dry conditions. For each pair of friction jaws 5 cleaned DC04 strips are drawn. A summary of the resulting friction coefficients is presented in Fig 16. The lowest friction occurs for the polished tools. A reason might be that the polished surfaces have less roughness peaks at which interlocking with the peaks of the strip topography is possible. Less ploughing of contacting asperities is the consequence. A distinctive difference between rough and smooth ground surfaces does not appear. The highest friction coefficients occur with friction jaws ground in drawing direction. Comparing the ground tools, grinding marks transversal to the drawing direction have a positive influence on the friction coefficient. A reason might be that due to the transversal grinding marks the direct contact between tool and strip is interrupted which leads to a reduction of adhesion. Furthermore, for transversal rough ground tools the true contact area is smaller compared to the tools ground smooth and in drawing direction. Hence, the target area for adhesion occurrence is reduced.

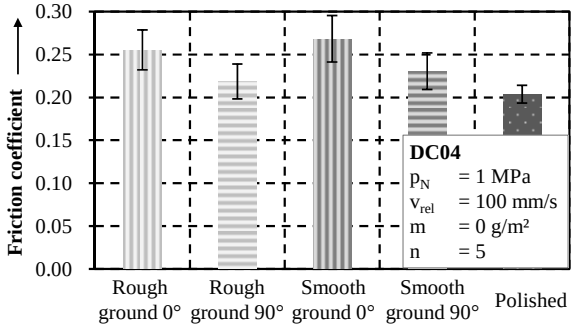

Fig. 16: Friction coefficients for DC04 strips under dry conditions

These results show that the tool topography is an important parameter in dry tribological systems. Further studies with geometrically defined surface features are performed to understand how a patterned surface influences friction and wear.

4.2 Patterned surfaces

The generation of micro features on tool surfaces aims at the control of material flow. For this purpose, friction coefficients which are different from non-patterned and coated surfaces should be adjusted by micro features' properties.

4.2.1 Definition of feature properties

Prior to the investigation of the influence of micro features on ring surfaces on friction and wear by tribometer tests the feature properties have to be defined. Fig. 17 exemplarily shows a ring surface textured with rectangles. The feature geometry is defined by the width b, the length l and the feature depth t_F. These three variables eventuate in the feature volume V_F. The orientation of features ζ defines the angle between the direction of rotation and the front edge, shown in Fig. 17.

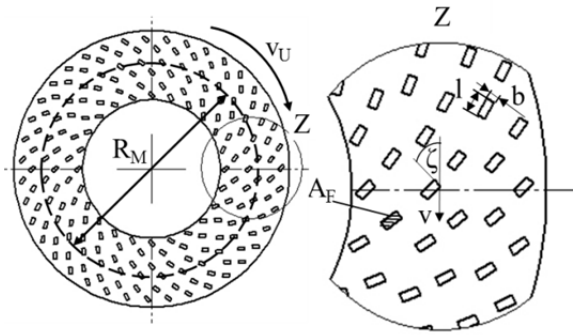

Fig. 17: Ring geometry and definition of the parameters of feature

The area coverage δ_F quantifies the ratio of the total feature surface area $A_{F,tot}$ and the area of the ring surface A_R, as described by eq. (2), where N_F labels the number of features.

$$\delta_F = A_{F,tot}/A_R = b \cdot l \cdot N_F/A_R \quad (2)$$

The variation levels of the feature properties are listed in Tab. 5.

Tab. 5: Feature properties for the reference (R1, R2), the preliminary (V1-V4) and the main experiments (H5-H16) according to Shainin. Each test was carried out with n= 3.

Test number	Feature shape	Width b in µm	Length l in µm	Feature depth d_F in µm	Area coverage δ_F in %	Orientation ζ
R1	dry, uncovered by features					
R2	lubricated, uncovered by features					
V1	rectangular	250	500	10	25	45°
V2	rectangular	250	500	10	25	45°
V3	square	100	100	5	10	90°
V4	square	100	100	5	10	90°
H5	rectangular	100	500	5	10	90°
H6	square	250	250	10	25	45°
H7	rectangular	250	500	5	25	45°
H8	square	100	100	10	10	90°
H9	rectangular	250	500	10	10	45°
H10	square	100	100	5	25	90°
H13	rectangular	100	500	10	25	45°
H14	square	250	250	5	10	90°
H15	rectangular	250	500	10	25	90°
H16	square	100	100	5	10	45°

These levels are chosen in relation to published results of investigations on micro features' effects on friction and wear. Segu et al. show the influence of different feature properties on dry friction [13]. In pin-on-disc configuration squared, circular and triangular features with dimensions between 250 µm and 500 µm are tested in [13]. Beneficial effects regarding lower friction coefficient and less wear were observed in dry sliding of steel surfaces on patterned surfaces compared to non-patterned surfaces.

4.2.2 Generation and analysis of micro features

The micro features are generated by ultrashort pulsed laser structuring with the laser system Fuego from the company Time-Bandwidth Products AG. This system provides pulse duration of 10 ps, a maximum average power of 42 W at a pulse frequency of 0.2 MHz and a wavelength 1064 nm. The laser beam is deflected on the sample surface by means of the galvanometer scanner hurryScan14 from the company Scanlab AG. Using f-theta lens with a focal length 160 mm, the spot diameter amounts 32 µm. Picosecond laser structuring is applied because of its advantages with regard to high dimensional accuracy and negligible dimensions of heat-affected zones [14].

The application of a peak fluence of Φ_0= 0.80 J/cm² at the pulse frequency of f_P= 200 kHz enables a high feature quality characterized by a height of existing burr smaller than 0.3 µm. This burr height corresponds to the mean surface roughness of the rings. For the generation of the micro features a scanning speed of v_x= 100 mm/s and a hatch line distance of p_y= 5 µm are applied. The feature depth of 5 µm respectively 10 µm is achieved by the application of N= 2 and N= 4 passes.

The samples are cleaned in an ultrasonic bath with isopropanol prior to laser treatment to enable constant absorption conditions. The cleaning step after laser treatment removes any debris from the ring surfaces. Both cleaning steps are necessary to ensure the repeatability of the tribological tests. Before and after the tribological tests the surface topography was measured by laser scanning microscope (LSM). This enables the evaluation of feasibility geometry of the different features, shown in Tab. 5, and of the wear volume.

4.2.3 Design of experiments for ring-on-disc tests

The first investigation step in ring-on-disc tests enables the identification of parameters which significantly influence friction and wear. For this purpose, screening experiments according to the Shainin variables search are carried out [15]. The Pareto concept has to be fulfilled as a condition for the applicability of the Shainin method. Because in [13] Segu et al. approved the existence of only few influencing parameters in tribological systems this condition is assigned. Thus, each two-level varied parameter is chosen with one setting each to provide low and high ring-on-disc friction coefficient μ_{rod}. Executing preliminary experiments twice the set levels - number V1 to V4 in Tab. 5 - should represent the correct choice of parameters due to the fulfillment of the criterion

D/d≥ 5 which can be calculated by eq. (3) according to Kleppmann [15]:

$$D/d= |(B1+B2)-(S1+S2)|/(|B1-B2|+|S1-S2|). \quad (3)$$

The variables B1, B2, S1 and S2 represent the Shainin coefficients which are the result out of the preliminary tests given in Tab. 6. Each feature property is varied towards both levels in these screening tests. The set levels for the numbers H5 to H16 are shown in Tab. 5 where the highlighted boxes mark the setting suggested to achieve low μ_{rod}. For evaluation and comparison purposes, tests with lubricated and dry surfaces without features (R1, R2) are carried out.

The second investigation step is used to vary the parameters identified as most significant to be able to adjust friction coefficient μ_{rod} and wear with regard to tailored surfaces.

4.2.4 Friction and wear in dry sliding of zinc-coated sheet surfaces on steel

Prior to the tests of patterned surfaces the methodology for the evaluation of the ring-on-disc tests is approved. The necessity of preliminary investigations and the adaption of the methodology is a consequence of the observed trend of the friction coefficient where no steady state as in usual tribological tests [16] can be chosen (Fig. 18). For preliminary and reference experiments a test duration of 300 s is chosen. This duration corresponds to a total mean sliding distance of approximately 31.5 m. The tests are carried out at a rotational speed of v_{rel}= 100 mm/s and a contact pressure of p_N= 2.1 MPa as these parameters are also applied in the following ring-on-disc tests. This chosen contact pressure represents a load condition which is similar to these at the blank holder in deep drawing processes of steel [12].

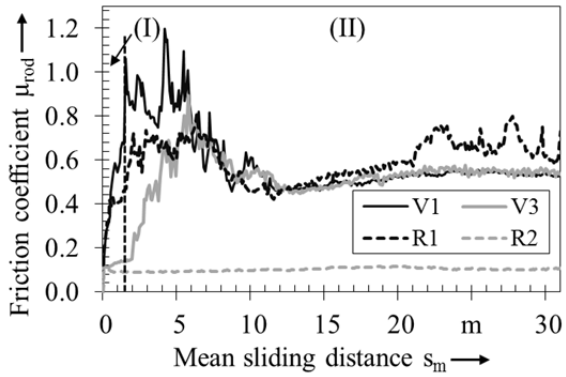

Fig. 18: Exemplary friction coefficient μ_{rod} depending on the mean sliding distance for patterned (V1, V3) and non-patterned, dry tribological pairings (R1) and the lubricated reference (R2)

The friction coefficient μ_{rod} measured in these experiments is exemplarily shown by Fig.18. The friction coefficient in dry sliding obviously reaches a higher value than the lubricated R2. Due to the direct contact of tool steel 1.2379 and the zinc layer covering the DC04 disc adhesive and abrasive wear of the zinc layer occurs. This observation can be explained by the existence of adherence on the ring and ridges on the disc. The steep rise of μ_{rod} in regime (I) in Fig. 18 is caused by adhesive wear characterized by adherence of zinc on the ring surfaces. Galling is one reason for this adherence [17]. At the beginning of regime (II) friction coefficient starts to fluctuate and high absolute values for μ_{rod} are reached. This fluctuation already starts after a mean sliding distance s_m= 0.8 m, occasionally. At this point the ring surface partially begins to slide on DC04 material of the disc. This assumption is justified by the observable dark patches after the total mean sliding distance $s_{m,tot}$= 2.0 m in Fig. 19. Furthermore, the strong fluctuation of μ_{rod} and even higher absolute values of μ_{rod} than in the tests against zinc-coated discs are observed in ring-on-disc tests of 1.2379 on pickled DC04. Due to adhesive and abrasive wear and the succeeding fluctuation no steady state of μ_{rod} as in common tribological tests [16] occurs.

The lifetime of the zinc layer and consequently the lifetime of the tribological system 1.2379/zinc are investigated by additional ring-on-disc-tests. The lifetime is given by the interval in which the zinc-layer completely covers the DC04 sheet without any hole. Rotating each ring against one disc the total mean sliding distance is varied. Fig. 19 shows three discs after different total sliding distances. The width of the wear track rises due to the increase of material transfer from the zinc-layer on the ring surface. This increasing material transfer is caused by decreasing galling resistance due to higher temperatures at the surfaces of the tribological pairing. The number and size of the dark patches also increases for longer sliding distances. These patches indicate holes in the zinc layer uncovering the DC04 which are generated by adhesive wear and result from the inhomogeneous thickness of the zinc layer. Only few small holes are visible at a sliding distance below 2 m caused by the stochastic process of the hole generation and inhomogeneous bursting of the zinc layer. Thus, no contact of 1.2379 and DC04 can be assumed which implies the tribological system consisting constantly of 1.2379 and zinc.

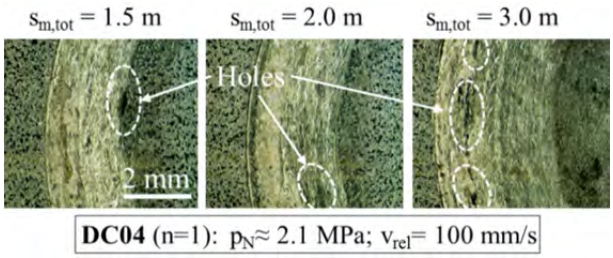

Fig. 19: Top views of different DC04 discs after different total sliding distances $s_{m,tot}$

The method for tribological investigation is adapted according to the following restrictions. Common deep-drawing processes imply a distance of the punch of approximately 0.3 m [12]. The sliding distance Δs_m= 0.5 m is selected which equals nearly twice this punch distance. This distance enables a maximum sliding distance as well as the constant tribological system 1.2379/zinc. The acceleration of the rotating ring takes nearly 0.3 m. Thus, the regime (I) which is

relevant for evaluation starts at a mean sliding distance of 0.3 m. It ends at s_m= 0.8 m regime (II). The distinguishing between both regimes is necessary because of the different tribological systems. In case of regime (II) the system partially consists of the pairing 1.2379/DC04 and 1.2379/zinc instead of 1.2379/zinc which only exists within regime (I). The regime (I) is evaluated in terms of the following variables in the case of non-patterned and patterned ring surfaces:

- The controllability of the forming process is assessed by the slope of the friction coefficient $m_{\mu rod}$. A process, in which the friction depending on a limited sliding distance is nearly constant and predictable, is characterized by a lower slope. In lubricated experiments this slope is almost zero within regime (I).
- The defined adjustment of μ_{rod} respectively μ to obtain tailored surfaces is enabled by the evaluation of the average friction coefficient μ_{rod} within regime (I). In case of a small $m_{\mu rod}$, this parameter is meaningful.
- Supporting a meaningful value of μ_{rod} a small standard deviation of μ_{rod} is also preferred.

4.2.5 Effects of micro features on surfaces of 1.2379 against zinc coated DC04

The preliminary experiments of the screening tests are carried out to approve the existence of only few significant parameters influencing the slope of the friction coefficient $m_{\mu rod}$ respectively the main friction coefficient μ_{rod} according to Shainin [15]. Tab. 6 shows the results of $m_{\mu rod}$ for the preliminary experiments V1 and V2 (high μ_{rod}, high $m_{\mu rod}$) as well as V3 and V4 (small μ_{rod}, small $m_{\mu rod}$). According to eq. (3) the Shainin coefficient D/d=14> 5, so the chosen levels fulfill the criterion.

Tab. 6: Variance of the slope of the friction coefficient $m_{\mu rod}$ within regime (I)

Shainin coefficients	Corresponding test number	Slope of friction coefficient $m_{\mu rod}$
B1 [1/m]	V3	0.029
B2 [1/m]	V4	0.027
D [1/m]		0.670
S1 [1/m]	V1	0.650
S2 [1/m]	V2	0.750
d [1/m]		0.048
D/d		14

Therefore, the main screening experiments are evaluated to identify the significant feature properties influencing $m_{\mu rod}$ and μ_{rod}. In comparison to the lubricated reference test R2 which reaches steady state at $\mu_{rod} \approx 0.10$ and a slope of almost zero every dry experiment (except of H15) shows a higher $m_{\mu rod}$. The dry non-patterned reference R1 indicates an increase of μ_{rod} within regime (I) similar to the patterned samples. The higher slope in dry ring-on-disc-tests is caused due to adhesive and abrasive wear of the zinc-layer as described in chapter 4.2.4.

Fig. 20 illustrates the slope of friction coefficient $m_{\mu rod}$ measured for the patterned surfaces. To support visualization of conversion due to the change of a single feature property the average of the preliminary experiments of both levels (V1 to V4) is included. Evaluating the slope of the different friction coefficient trends of the patterned samples within regime (I) a distinct conversion of $m_{\mu rod}$ can be observed for the tests H15 and H16. According to Shainin Fig. 20 visualizes the significant influence of the varied parameter - the feature orientation - on $m_{\mu rod}$. The orientation ζ= 45° (H16) shows significantly higher $m_{\mu rod}$ than the second level ζ= 90° (H15). Thus, the feature orientation is a dominant parameter influencing the slope of friction coefficient (so-called 'Red X' according to Shainin [15]).

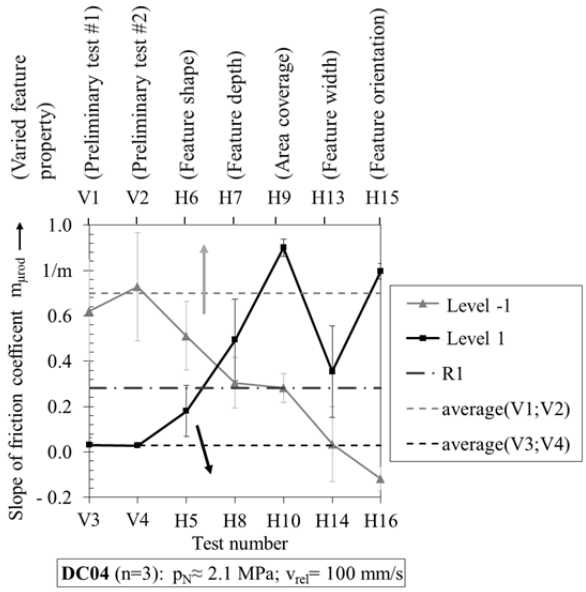

Fig. 20: Slope of the friction coefficient $m_{\mu rod}$ within regime (I) for the different feature properties - varied at two levels - as well as the non-patterned reference R1

The area coverage by the features δ_F is a less dominant parameter or has a strong interaction with another parameter (so-called 'Pink X') which is indicated by the test numbers H9 and H10 in Fig. 18. However, Segu et al. have determined the area coverage as the dominating influence on friction coefficient in dry pin-on-disc-tribotests of two hardened steels 100Cr6 [13]. The screening results show that the lower area coverage δ_F= 10% yields on lower $m_{\mu rod}$ than the second set level δ_F= 25%. The slope of friction coefficient is marginally influenced by the feature depth (H7, H8) and the feature width (H13, H14) because the reversion of both properties does not exceed the average low and high level of the preliminary tests V1 to V4. The feature shape (H5, H6) does not show any relevant influence on $m_{\mu rod}$. Regarding the significance of the feature properties' influence, the given statements pertain for micro features with lateral dimensions in the investigated range between 100 µm and 500 µm.

Evaluating the mean friction coefficient μ_{rod} within regime (I) - according to the same methodology of Shainin - the observable unilateral reversion indicates less dominant parameters: feature orientation, area coverage and feature depth. The screening results show that the lower area coverage δ_F= 10% yields on lower $m_{\mu rod}$ than the second set level δ_F= 25%. A variation of the feature orientation enables a lower $m_{\mu rod}$ at a higher

orientation angle. Also a higher mean friction coefficient is measured for the orientation $\zeta = 90°$. This result coincides well with the results observed by Xing et al. [18]. One reason of this result might be elastic and plastic deformation as well as galling of asperities influenced by the edges of the micro features [19]. This effect has to be investigated in further experiments.

Based on the results of the screening experiments the parameters significantly influencing friction and wear are varied in more detailed manner in the second step while the less significant parameters are set constant. Also, the feature orientation is chosen constantly to $\zeta = 90°$ to adjust a lower $m_{\mu rod}$. Additionally, an orientation perpendicular to rotation direction results in a smaller standard deviation of μ_{rod} than for $\zeta = 45°$. Thus, the area coverage is varied in three steps under the constraints of the chosen feature properties given in Fig. 21. Rectangular feature shape as well as feature depth $t_F = 5$ µm are chosen.

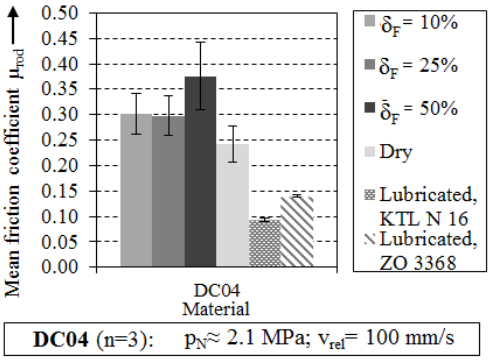

Fig. 21: Mean friction coefficient μ_{rod} depending on the area coverage ρ_F on patterned surfaces and non-patterned dry and lubricated reference tests

The comparison of the determined friction coefficients shows an increase of μ_{rod} as well as an increase of standard deviation by significantly rising area coverage from $\delta_F = 25\%$ to $\delta_F = 50\%$. Each patterned surface results in a higher μ_{rod} than the dry reference while the lowest mean friction coefficients are realized by the lubricated reference tests.

This dependence of μ_{rod} on the area coverage can be explained by the increasing contact pressure because of decreasing contact area. The higher contact pressure induces more intensive interaction between the friction partners characterized by interlocking, plastic deformation and galling of asperities. These mechanisms result in higher adhesive wear. Increasing adhesion might be one reason of the observed higher slope $m_{\mu rod}$ for $\delta_F = 25\%$ compared to $\delta_F = 10\%$. Furthermore, increase of the friction coefficent μ_{rod} by increasing area coverage can also be caused due to rising adhesion affinity. The increase of adhesive wear of the zinc layer can be confirmed by the measured volume of adherence V_A (Fig. 23(a)).

On each ring the volume below and above the ring surface (Fig. 22 (b)) is measured within the region of interest (ROI) to measure the different volumes of wear. The ROI shown in Fig. 22 (a) measures approximately 4.66 mm by 0.6 mm which corresponds to the ring width times the size of one field of measurement at 20-fold magnification of the used laser scanning microscope. The volume of trapped wear particles V_P is calculated by the difference of the volume below the surface before and after tribotests (Fig. 22 (b)).

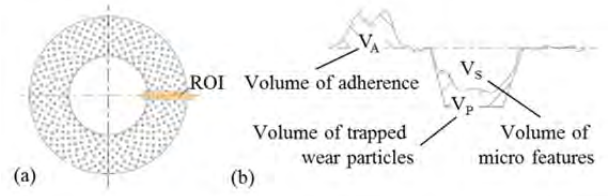

Fig. 22: (a) Location of region of interest for the measurement (b) of different volumes above and below the ring surface

Wear volume is determined twice on each ring. Each measurement is carried out at the locations of maximum and minimum adherence.

The volume of adherence V_A as well as the filled volume of micro features V_P show a rise for increasing area coverage in Fig. 23 (a) and (b).

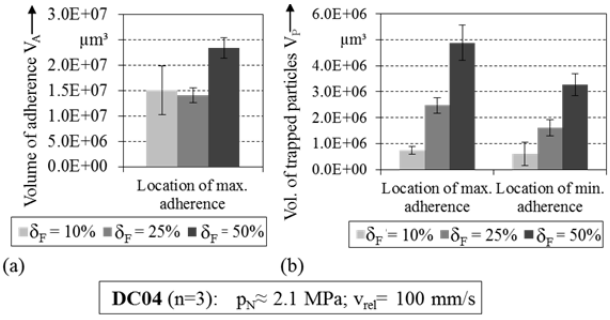

Fig. 23: (a) Wear volume of the ring surfaces resulting from adherence and (b) volume of trapped wear particles

These trends of the wear volume of the ring surfaces are illustrated by the top-views of the rings in Fig. 24. The sequences of ring surfaces show a larger area of adherence with rising area coverage. Each of the ring samples is tested on four discs. The features with higher area coverage are filled to a bigger part at the outer ring of the surface, as shown by Fig. 24.

This impression is confirmed by the measured volume of trapped particles V_P. Fig. 23 (b) indicates an increasing amount of wear particles trapped by features at increasing area coverage due to the doubled volume V_P.

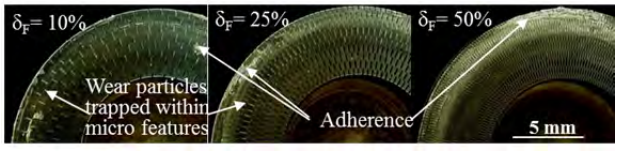

Fig. 24: Top view of ring surfaces after ring-on-disc tests on DC04 with adherence and micro features filled by wear particles ($p_N \approx 2.1$ MPa; $v_{rel} = 100$ mm/s; $s_{m,tot} = 6.0$ m)

Eventually, the effects of micro features on friction and wear can be explained by some basic approaches. In general, the micro features act as a trap for wear particles and are mainly filled by zinc within a very short mean sliding distance as shown in Fig. 24. This trapping can stabilize the trend of friction coefficient due to the prevention of ploughing of the zinc layer [13]. The applied micro features also reduce contact

area. Thus, the contact pressures change and interlocking of asperities affects a higher friction coefficient due to adhesion. Trapping of wear particles might also influence adhesion affinity because the direct contact of the same material of the captured particles and the sheet respectively work piece increases adhesion affinity. Thus, friction coefficient and wear of the zinc layer increase. In the case of elastic deformation of the zinc layer due to high contact pressures the feature edges can influence abrasive wear and galling [19]. Each of the proposed mechanisms which influence friction and wear has to be investigated in further experiments.

4.3 Coated Surfaces

Former Former studies have shown that applying DLC coated tool surfaces can significantly reduce friction and wear. Weihnacht et al. [20] have proofed a positive tribological behavior of ta-C coatings for dry forming aluminum alloys. Further studies reveal a general applicability of DLC coatings for dry forming processes [21]. Therefore, another kind of surface modification within this project is realized with DLC coatings which seem to have preferable properties under dry conditions.

A series of a-C:H:W coatings were deposited on flat discs and rings from tool steel 1.2379, hardened and tempered to 60 ± 1 HRC. Before loading the deposition chamber the specimens were ultra-sonically cleaned in acetone and in isopropanol and after that dried using nitrogen. Prior to the deposition process the substrates were plasma etched by a bombardment of argon ions, in order to remove contaminants and stored gas molecules from the surface. The coating system, including an adhesive layer of chromium, an interlayer of tungsten carbide and a functional layer of a-C:H:W, was deposited by using a hybrid PVD/PECVD coating machine (H-O-T., TT-300) and a twofold rotating charging rack. As coating technologies arc evaporation and unbalanced magnetron sputtering were used for the Cr adhesive layer and the WC interlayer, respectively. The a-C:H:W functional layer was deposited by reactive unbalanced magnetron sputtering of a binder-free WC target using MF power supply (40 kHz, pulse width 5 µs) in an argon-acetylene atmosphere. The substrate bias voltage U_{bias} and the argon flow ϕ(Ar) during the deposition process are listed in Tab. 7.

Tab. 7: Process parameters (factors) for the deposition of different a-C:H:W coating samples

Sample	U_{bias} in V	Φ(Ar) in sccm	$P_{sputter}$ in kW	$Φ(C_2H_2)$ in sccm
S01	203	128	1.4	40
S02	57	232	1.4	40
S03	130	180	1.4	40
S04	203	232	1.4	40
S05	57	128	1.4	40

Fig. 25 (a) shows a representative a-C:H:W coated surface. It can be seen that there are some small to very large spots distributed on the surface. Most of them are peaks according to the surface height information (see Fig. 25 (b)) measured by laser scanning microscope. A FIB cross section of the a-C:H:W coating system with a thin Cr adhesive layer is shown in Fig. 25 (c). The a-C:H:W layer exhibits a typical columnar structure [16], [22]. Due to the extremely high power density during the arc process the Cr target material was evaporated in a mixture of charged ions, neutral particles, clusters and macro-particles. Especially the macro-particles, the so called “droplets”, result in increasing number of peaks on the coating surface.

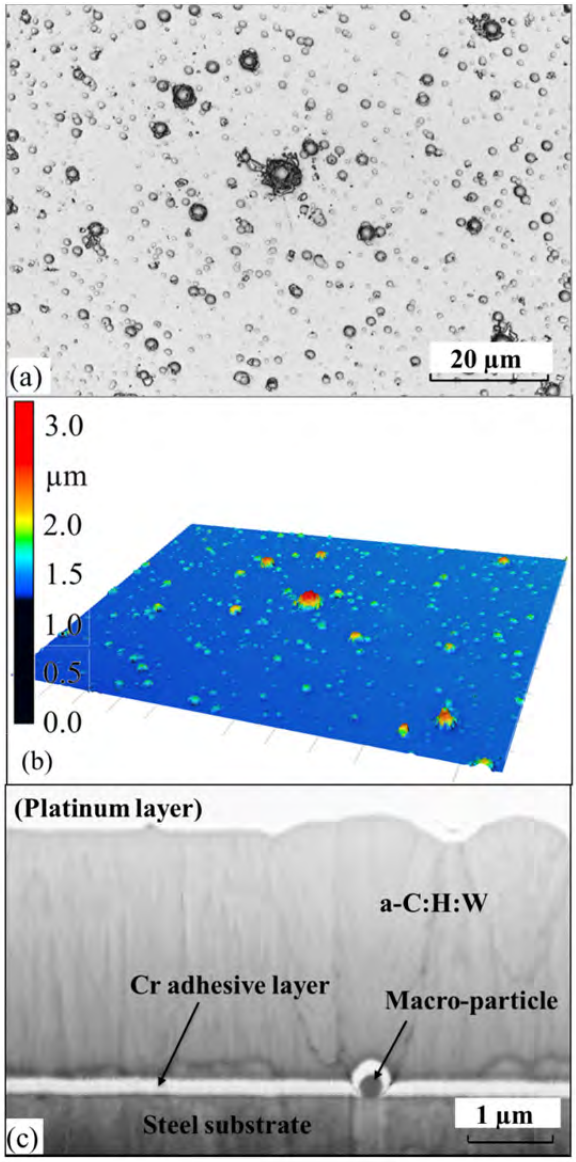

Fig. 25: Microscopic investigations of a typical a-C:H:W coated surface: (a) Surface topology, (b) Height information and (c) SEM images of a FIB cross section

The total thickness of the coating system, including the Cr adhesive layer, the tungsten carbide interlayer and the a-C:H:W functional layer, is in the range of 2.1 to 2.8 µm. The coatings have generally adhesion strengths between HF classes 2 to 4, which are acceptable according to [23]. The Martens hardness HM at indentation depth of about 200 nm has been considered as the coating hardness according to Bückle’s rule [24]. The five different coating samples exhibit various hardness HM from 5.6 to 8.1 GPa. The elastic indentation modulus E_{IT} of the five coating

variants measured at 25 points vary from 135 to 162 GPa.

The different a-C:H:W coating variants were tested without any post-treatment of the surfaces using the ring-on-disc-tribometer. The mean friction coefficient against deep drawing steel DC04 is presented in Fig. 26. Under dry sliding conditions μ_{rod} varies from 0.5 to 1.1. μ_{rod} represents the mean value from 2.5 to 10 meters sliding distance. As shown in Fig. 26, all a-C:H:W coating variants show remarkably higher friction coefficients compared to that of the uncoated 1.2379/DC04 dry contact. The extremely high friction coefficients are significantly associated with the transfer of the zinc, perhaps also steel, on the DLC coated surface, led to strong abrasive wear on the steel sheet, which caused steel/steel contact since the DLC coating is covered by steel adhesion.

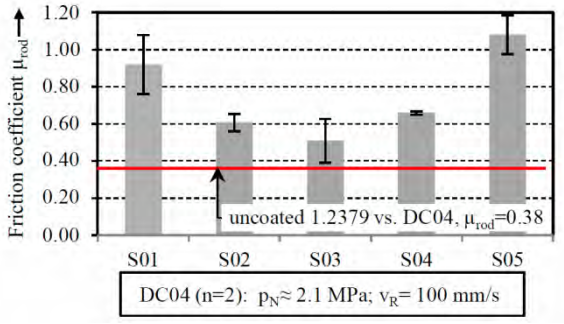

Fig. 26: Friction coefficients of different a C:H:W variants (rings) against DC04 (discs) in the ring-on-disc-test under dry conditions.

Fig. 27 shows the wear tracks on the DLC rings and their counter bodies. After 10 s testing time the zinc layer began to transfer on the DLC coated ring and adhesion was detected on the DLC coating. After 100 s testing time the zinc adhesion on the coating was extinct. Instead, two areas were distinguished: the smooth outer ring area and the rough inner ring area.

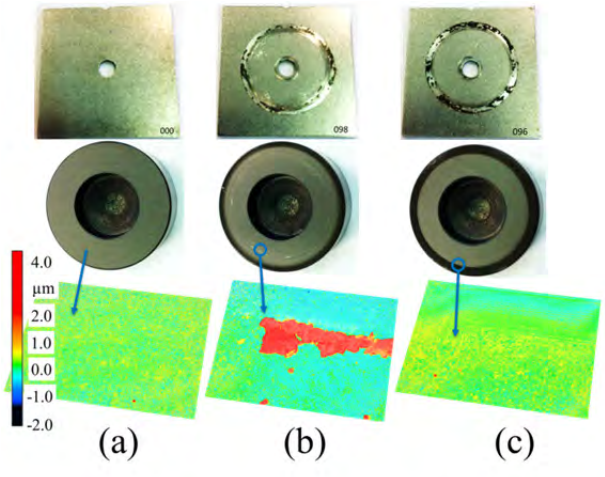

Fig. 27: Wear tracks and height information of (a) original coated surface, (b) coated surface after 10 s sliding and (c) coated surface after 100 s sliding

Fig. 28 describes two main wear processes which occur during the ring-on-disc tests. In the initial state the coated ring rotates over the fixed DC04 disc. The zinc layer starts to transfer on the coating in the first phase. This phenomenon usually begins at the outer ring track because of the higher sliding speed. As shown in Fig. 28, the coating material is transferred back to the sheet. Thus, in the second phase two areas can be distinguished: The outer ring area, where typically a smoothed surface can be found and the inner ring area, where the surface does not change significantly. The materials transfer on each other led to material pile-up on the sheet surface, which results in a reduction of the real contact area.

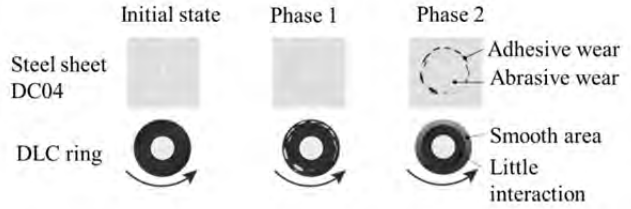

Fig. 28: Schematic of the wear process for DLC coated samples and their counter bodies of DC04 sheet steel in the ring-on-disc-test

The extremely high friction coefficient of the a-C:H:W coatings against DC04 is also to be associated with an increasing surface roughness through increasing surface asperities during the deposition process. The R_z of all coatings after deposition process were measured up to 1.9 µm, which is about double the roughness of the original steel substrate (R_z: 0.8 µm to 1.0 µm). Especially asperities in the surface topography are disadvantageous, which led to R_{pk} up to 0.68 µm (uncoated surface: R_{pk} from 0.09 µm to 0.12 µm). To investigate the effect of these surface asperities to dry friction, three of the coatings (S01, S03, S05) were chosen to be polished by using a diamond suspension (1 µm), resulting in a comparable roughness of the uncoated steel substrate (R_z = 0.8...1.2 µm and R_{pk} = 0.18…0.20 µm). As shown in Fig. 29 the friction coefficient was reduced significantly by this surface treatment. Especially for the coating variants S03 and S05 the friction coefficient decreases to about 0.25 after a short running-in phase.

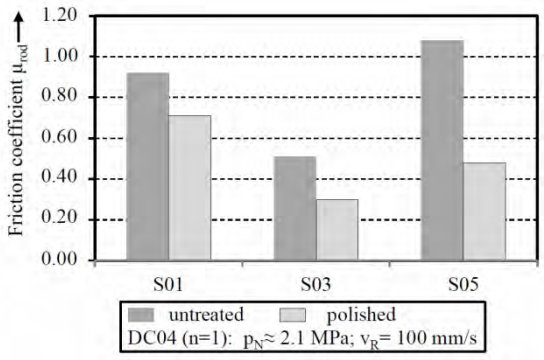

Fig. 29: Friction coefficient vs. sliding distance of coated samples, original and polished

5 Summary and Outlook

This paper presents first results regarding development and design of tailored surfaces for the realization of dry deep drawing processes. Reference experiments in terms of strip drawing tests and surface characterization show huge increase of friction and wear

under lubricant free conditions. Dry friction coefficients μ vary between 0.15 and 0.6 depending on sheet material. To design the forming process a forming simulation of deep drawing of a rectangular cup is modelled. The critical tool segments and influencing process parameters are investigated by variant simulation. Results show that for realizing dry forming, surface modifications are required especially in the die radius and in the case of using aluminum alloys.

Micro features on the tool surfaces are one opportunity to realize tailored surfaces. Therefore, the features' effects are investigated in tribometer tests. According to developed assessment criteria for the trend of friction coefficient - depending on the endurance of the zinc layer covering DC04 discs - feature properties are identified which significantly influence friction. Under the constraint of constant feature orientation $\zeta = 90°$ the increase of area coverage by micro features causes higher friction coefficient as well as higher wear due to adhesion. In order to control the material flow higher friction can be adjusted by setting the area coverage of micro features on tool surfaces in comparison to non-patterned surfaces. This parameter has carefully to be chosen because of higher adhesive wear.

The results of untreated and polished surfaces which are coated by a-C:H:W show that post-treatment of DLC surface is necessary to reduce asperity heights before it is applied for forming operations. To further reduce adhesive wear and metal material transfer, the coating deposition recipe will be improved by doping with additional elements. Further investigations need to be done in order to understand the basic tribological mechanisms of the coating and workpiece interaction under dry conditions. Experiments with various coating properties will be performed to identify the main adjusting parameters for coating development and design for dry deep drawing processes. An increasing understanding for developing tailored surfaces will eventually enable the realization of dry deep drawing processes.

Acknowledgement

The authors thank the German Research Foundation (DFG) for supporting the presented investigations by funding the priority program SPP 1676 project ME 2043/43-1, SCHM 2115/36-1 and TR 1043/1-1 with the project title "Lubricant free forming with tailored tribological conditions".

References

[1] F. Vollertsen, F. Schmidt: Dry Metal Forming: Definition, Chances and Challenges. Int. J. Precision Engineering and Manufacturing – Green Technology 1/1 (2014) 59-62

[2] E. Doege, K.-P. Witthüser, R. Grahnert: Untersuchung der Reibungsverhältnisse beim Tiefziehen. In: Tribologie: Reibung, Verschleiß, Schmierung. Berlin: Springer, 1981

[3] M. Meiler, H. Jaschke: Lubrication of Aluminium Sheet Metal within the Automotive Industry. Advanced Materials Research 6-8 (2005) 551-558

[4] A. Matuszak: Factors influencing friction in steel sheet forming. Journal of Materials Processing Technology 106 (2000) 250-253

[5] E.D. Szakaly, J.G. Lenard: The effect of process and material parameters on the coefficient of friction in the flat-die test. Journal of Materials Processing Technology 210 (2010) 868–876

[6] M. Jałbrzykowski: An investigation into the mechanisms of wear of zinc from the surface of zinc-coated car-body sheets during friction. Wear 303 (2013) 519–523

[7] K.R. Sriraman, H.W. Strauss, S. Brahimi, R.R. Chromik, J.A. Szpunar, J.H. Osborne, S. Yue: Tribological behavior of electrodeposited Zn, Zn–Ni, Cd and Cd–Ti coatings on low carbon steel substrates. Tribology International 56 (2012) 107–120

[8] L. Kirkhorn, K. Frogner, M. Andersson, J.E. Ståhl: Improved Tribotesting for Sheet Metal Forming. Procedia CIRP 3 (2012) 507–512

[9] J. Coello, V. Miguel, A. Martínez, F.J. Avellaneda, A. Calatayud: Friction behavior evaluation of an EBT zinc-coated trip 700 steel sheet through flat friction tests. Wear 305 (2013) 129-139

[10] F. Barlat, J. Brem, J. Yoon, K. Chung, R. Dick, D. Lege, F. Pourboghrat, S.-H. Choi, E. Chu: Plane stress yield function for aluminum alloy sheets—part 1: theory. International Journal of Plasticity 19 (2003) 9, 1297–1319

[11] F. Quetting, P. Hora, K. Roll: Modelling of Strain Hardening Behavior of Sheet Metals for Stochastic Simulations. Key Engineering Materials 504-506 (2012) 41-46

[12] A. Birkert, S. Haage, M. Straub: Umformtechnische Herstellung komplexer Karosserieteile. Berlin: Springer, 2013

[13] D.Z. Segu, J. Kim, S.G. Choi, Y. Jung, S. Kim, Application of Taguchi techniques to study friction and wear properties of MoS2 coatings deposited on laser textured surface, Surf. Coat. Technol. 232 (2013) 504-514

[14] T. Häfner, Y. Reg, H. Hetzner, M. Schmidt: Microstructuring Tools for Sheet Bulk Metal Forming - A Designated Application for Picosecond Laser. J. Laser MicroNanoen. 8 (2013) 39-44

[15] W. Kleppmann, Taschenbuch Versuchsplanung, 7th ed., Hanser, München, 2011

[16] H. Hetzner, R. Zhao, S. Tremmel, S. Wartzack: Tribological adjustment of tungsten-modified hydrogenated amorphous carbon coatings by adaption of the deposition parameters. Proc. 10th Int. Conf. THE "A" Coatings in Manuf. Eng. (2013) 39-49

[17] C.N. Panagopoulos, K.G. Georgarakis, P.E. Agathocleous: Sliding wear behaviour of Zinc–Nickel alloy electrodeposits. Tribol. Int. 36 (2003) 619-623

[18] Y. Xing, J. Deng, Z. Wu, H. Cheng: Effect of regular surface textures generated by laser on tribological behavior of Si3N4/TiC ceramic, Appl. Surf. Sci. 265 (2013) 823-832

[19] B. Podgornik; J. Jerina: Surface topography effects on galling resistance of coated and uncoated tool steel. Surface and Coatings Technology 206 (2012) 11-12, 2792-2800

[20] V. Weihnacht, A. Brückner, S. Bräunling: ta-C beschichtete Werkzeuge für die Trockenumformung von Aluminiumblechen. Vakuum in Forschung und Praxis. 20 (2008) 3 6-10

[21] K. Taube: Carbon-based coatings for dry sheet-metal working. Surface and Coatings Technology 98 (1998) 1-3 976-984

[22] Association of German Engineers (VDI) VDI Guideline 2840. Berlin: Beuth, 2012

[23] Association of German Engineers (VDI) VDI Guideline 3198. Berlin: Beuth, 1992

[24] G. Berg, P. Grau: Influence of the Substrate Hardness on the Validity of Bückle's Rule. Cryst. Res. Technol. 28 (1993), 989-994